PhD TUTORIAL

Chaos synchronization in a mutually coupled laser array subjected to self-mixing modulation

R Kawai[1,5], J-S Lih[2], J-Y Ko[3], J-L Chern[4] and K Otsuka[1]

[1] Department of Human and Information Science, School of Information Technology and Electronics, Tokai University, 1117 Kitakaname, Hiratsuka, Kanagawa 259-1292, Japan
[2] Department of Physics, National Cheng Kung University, Taiwan 70101, Taiwan, Republic of China
[3] Department of Physics, National Kaohsiung Nomail University, Kaohsiung 802, Taiwan
[4] Department of Electro-Optical Engineering, National Chiao Tung University, 1001 Ta-Hsuen Road, Hsinchui, Taiwan 30050, Taiwan

Abstract
This tutorial presents a detailed description of experiments, simulations, and characterizations of chaos synchronization phenomena in the model of a mutually coupled microchip solid-state laser array subjected to self-mixing feedback modulation. We demonstrate a transition to synchronized chaos by the method of 'phase squeezing' with increasing field overlap between the two lasers. This phenomenon is well reproduced by numerical simulation of model equations. It is also shown that low energy variation as well as high disorder are concurrently established in synchronized chaos in the present system. The deterministic random switching (i.e., chaotic itinerancy) among phase-squeezed states and synchronized chaos states is numerically demonstrated in a transition region from a phase-squeezed state to a synchronized state. We characterize observed behaviours using such methods as singular value deposition (SVD), joint time–frequency analysis (JTFA) introducing a similarity function, and coarse-grained information transfer rate (CITR) analysis of long-term experimental or numerical time series, and discuss the physical significance of observed nonlinear dynamics in conjunction with chaos synchronization in mutually coupled lasers.

Keywords: microchip laser array, self-mixing modulation, chaos synchronization, phase-squeezed state, statistical analysis, dynamical characterizations

1. Introduction

A recent study in nonlinear dynamics has revealed that two, or more than two, chaotic systems can be synchronized when they are coupled appropriately [1, 2]. This interesting phenomenon plays a key role in the chaotic dynamics of communication signals and may be applied to the real-time recovery of signals, which have been masked in a chaotic background, and thus to encoded communications [3]. In the context of interacting chaotic oscillators, there are different

[5] Permanent address: Hashimoto 7-14-9, Sagamihara, Kanagawa 229-1103, Japan.

interpretations of the 'synchronization', such as master–slave synchronization [2] and the synchronization based on mutually coupled oscillators [4, 5]. *Generalized chaos synchronization* based on generalized functional dependence between two different variables has also been included to reveal the dynamical correlations [6, 7]. On the other hand, a related chaos synchronization phenomenon can be developed in terms of a suitably defined 'phase' of a chaotic oscillator [8]. Chaotic amplitude fluctuation usually triggers a diffusion of phase. In the phase synchronization state, amplitudes of coupled oscillators remain chaotic but their phases are in step with a common timing characteristic. *Phase synchronization* could be an important consideration in schemes for communication using the natural symbolic dynamics of chaos [9]. The clock timing of information bits is typically a key factor in a communication system, so a termination of phase diffusion is crucial in an application to encoded communication. In contrast to phase synchronization, *lag* [10, 11] or *anticipated chaos synchronization* [12, 13] have been also demonstrated, in which amplitudes of two chaotic oscillators are correlated while their relative phase of amplitude fluctuations is shifted. Collective chaos synchronization has also been demonstrated experimentally in a modulated multimode laser, in which pair of modes exhibited phase, lag or generalized synchronization [14].

In this tutorial, detailed experimental results on chaos synchronization in a mutually coupled solid-state laser array subjected to delayed self-mixing laser-Doppler-velocimetry (SMLDV) modulation [15] are presented. An abrupt transition from unsynchronized chaos to synchronized chaos via a 'phase-squeezed state' is shown to take place when the field overlap (i.e., coupling) between the two lasers is increased. The phase-squeezed state is a dynamic state in which phase fluctuations of two lasers are squeezed reflecting the appearance of periodicities, while their amplitudes remain uncorrelated. Coupled laser array equations with self-mixing feedback are introduced and observed behaviours are reproduced numerically. Statistical properties of different dynamic states (i.e., unsynchronized, phase-squeezed, and synchronized states) are examined, and low energy variation as well as high disorder are shown to be concurrently established in the synchronized state. It is also shown numerically that a deterministic switching between phase-squeezed states and synchronized chaos states (i.e., chaotic itinerancy [16]) occurs at a critical coupling where a transition from phase squeezing to synchronization takes place.

Several characterization methods of chaos synchronization have been proposed, including amplitude, phase correlation plots, and other statistical quantities. Here, we examine two statistical characterization methods, singular-value deposition (SVD) [17] and joint time–frequency analysis (JTFA), featuring a similarity function [18], of long-term experimental time series. The proposed JTFA reveals not only the correlation of two chaotic signals on a joint time–frequency space but also the novel self-organized structure on a time-correlation portrait (phase retrieval) of two joint time–frequency patterns established in synchronization chaos. We show that a netlike structure, which reveals the establishment of phase relationship between two signals, appears as the system evolves into
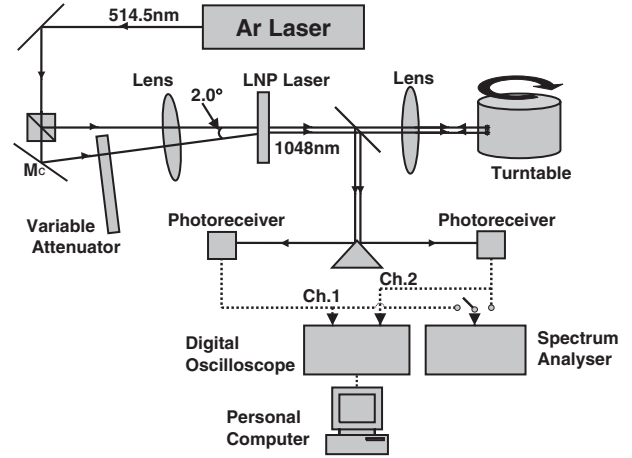

Figure 1. Experimental set-up of an LNP laser array subjected to Doppler-shifted optical feedback.

the phase-squeezing state, and finally a well organized self-similar structure obeying the power law is formed in a synchronized chaos state. Numerical chaotic itinerancy is characterized using information circulation [19–21] and dynamic change in transinformation rate (i.e., entropy) is shown to occur associated with switchings among different dynamic states.

2. Experimental results

2.1. Experimental scheme

The experimental system, in which we used an Ar-laser-pumped LiNdP$_4$O$_{12}$ (LNP) laser, is shown in figure 1. The output light was divided into two beams by the beam splitter and was focused on the input surface of the LNP crystal by a common focusing lens. The intensity of pump beam 2 was about three times that of beam 1 and was controlled by a variable attenuator. The end faces of the plane-parallel 1 mm thick LNP crystal were directly coated by dielectric mirrors, M$_1$ (transmission at pump wavelength $\lambda_p = 514.5$ nm: 80%; reflection at lasing wavelength $\lambda_l = 1048$ nm: 99.9%) and M$_2$ (transmission at λ_l: 1%). The stoichiometric LNP crystal has a Nd concentration which is 30 times higher than Nd:YAG and the absorption length at 514.5 nm is only 400 μm. Consequently, the pumping of laser 2 by oblique beam 2 resulted in only a slight increase in threshold pump power because of the pump-induced thermal lens effect. The threshold pump power P_{th} for both lasers was 120 mW, and linearly polarized TEM$_{00}$ oscillations were obtained. The spatial separation d of the pump positions of lasers 1 and 2 was larger than their pump beam spot size ($\simeq$40 μm) averaged over the absorption length. Therefore, cross-saturation of population inversions did not take place between the two lasers. The coupling between the two lasers occurred through the overlap of their lasing fields, whose spot sizes $w_l \simeq 200$ μm. The coupling coefficient, $|\eta| = \exp(-d^2/2w_l^2)$, is normalized so that $|\eta| = 1$ for $d = 0$ [5, 22]. At the separation of 0.8 mm used in this experiment, $|\eta|$ is estimated to be 3.35×10^{-4}. The separation d was varied precisely by tilting the mirror M$_c$ in figure 1. π out-of-phase locking was observed in the present system, so η can be considered to have a negative real value [22]. The two parallel beams
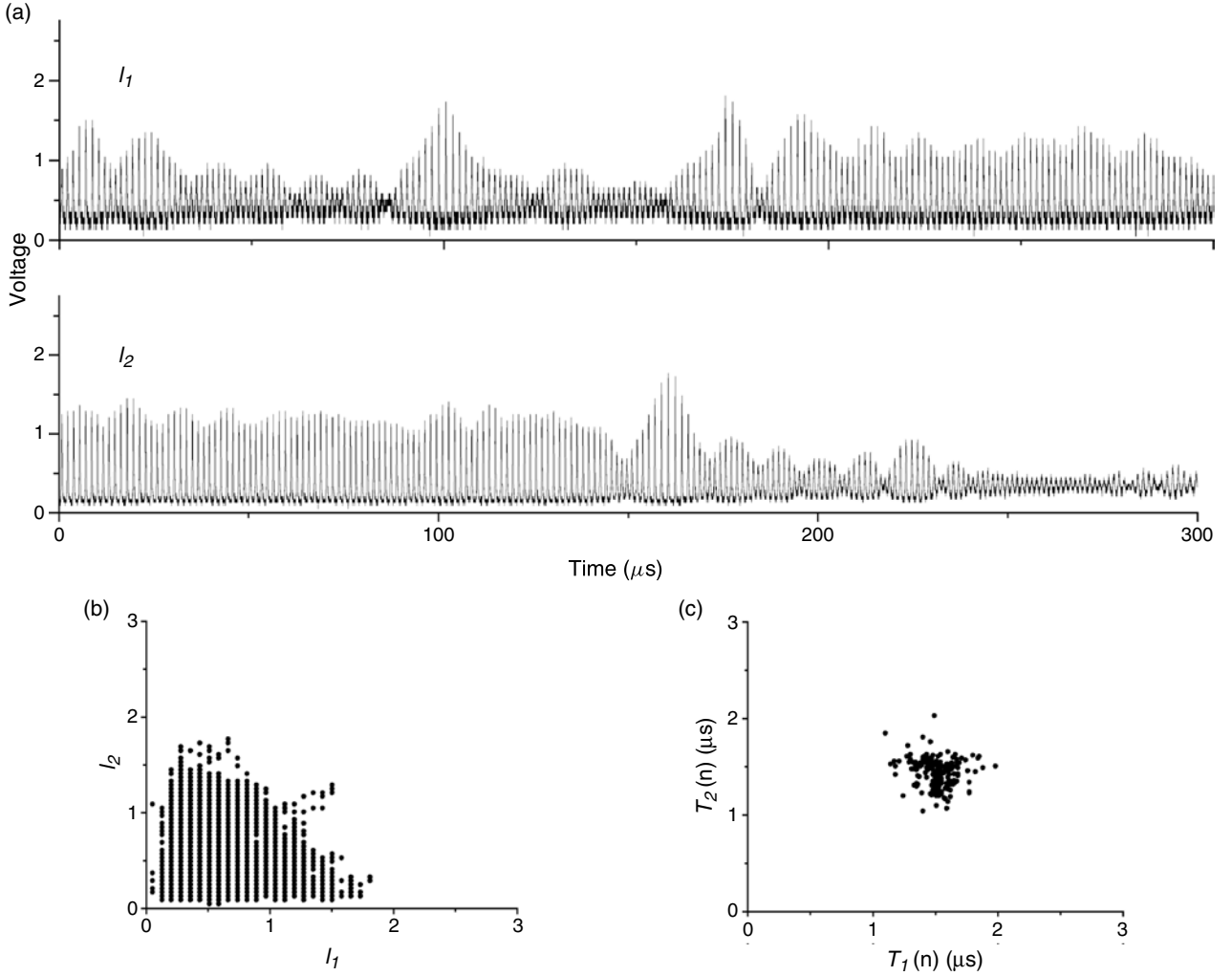
Figure 2. Experimental result of unsynchronized chaos. $d \simeq 1.5$ mm. (a) Time evolutions of two lasers, (b) amplitude correlation, and (c) phase correlation.

from the LNP laser were incident to and scattered from the turntable to modulate themselves by the SMLDV feedback, in which microcavity lasers are loss modulated equivalently because of the interference between the lasing and scattered feedback fields [23], which possess a narrow-band Gaussian frequency distribution, at the Doppler-shift frequency f_D. The distance between the LNP laser and the turntable was 50 cm. *The distinct difference between the present system and the pump (or loss) modulation scheme [5, 22] is that the self-mixing feedback modulation depends upon whether or not the two coupled lasers are locked and on each laser's own intensity. The perturbation to the laser system is unidirectional and no feedback action occurs in the usual pump (or loss) modulation scheme.* The two monitoring beams were converted to electrical signals by two InGaAs photoreceivers (New Focus 1811, bandwidth 125 MHz) and observed by using a digital oscilloscope (Tektronix 420A, bandwidth 200 MHz, 100 MS s^{-1} sampling). Time series consisting of 30 000 data points were analysed by using a personal computer. The rf spectrum analyser (Tektronix 2712) was used to monitor the power spectra of the two lasers. The far-field pattern and intensity profile were measured by

using a PbS infared television. When the distance between beams 1 and 2 was shortened, a two-lobed far-field pattern was observed, indicating π out-of-phase locking of two lasers similar to [22].

The following experiments were carried out in the single-longitudinal-mode oscillation regimes of both lasers. When the modulation frequency f_D was tuned to be near the relaxation oscillation frequency $f_R = (1/2\pi)\sqrt{(w-1)/\tau\tau_p}$, where $w = P/P_{th}$ is the relative pump, τ is the fluorescence lifetime, and τ_p is the photon lifetime, chaotic relaxation oscillations were easily obtained. Synchronization was obtained when the pump power of beam 2 was set so that the relaxation oscillation frequencies of the two coupled free-running lasers almost coincide, where $f_R \simeq 600$ kHz. Otherwise, synchronization did not occur.

2.2. Dynamic states for different transverse field overlaps

Figure 2(a) shows example experimental time series of laser 1 (intensity I_1) and laser 2 (intensity I_2) for $d = 1.5$ mm. The amplitude correlation plot is shown in figure 2(b). To examine the phase correlation of the chaotic pulsations, the time interval between the nth peak and the subsequent peak

(a)

(b)

(c)
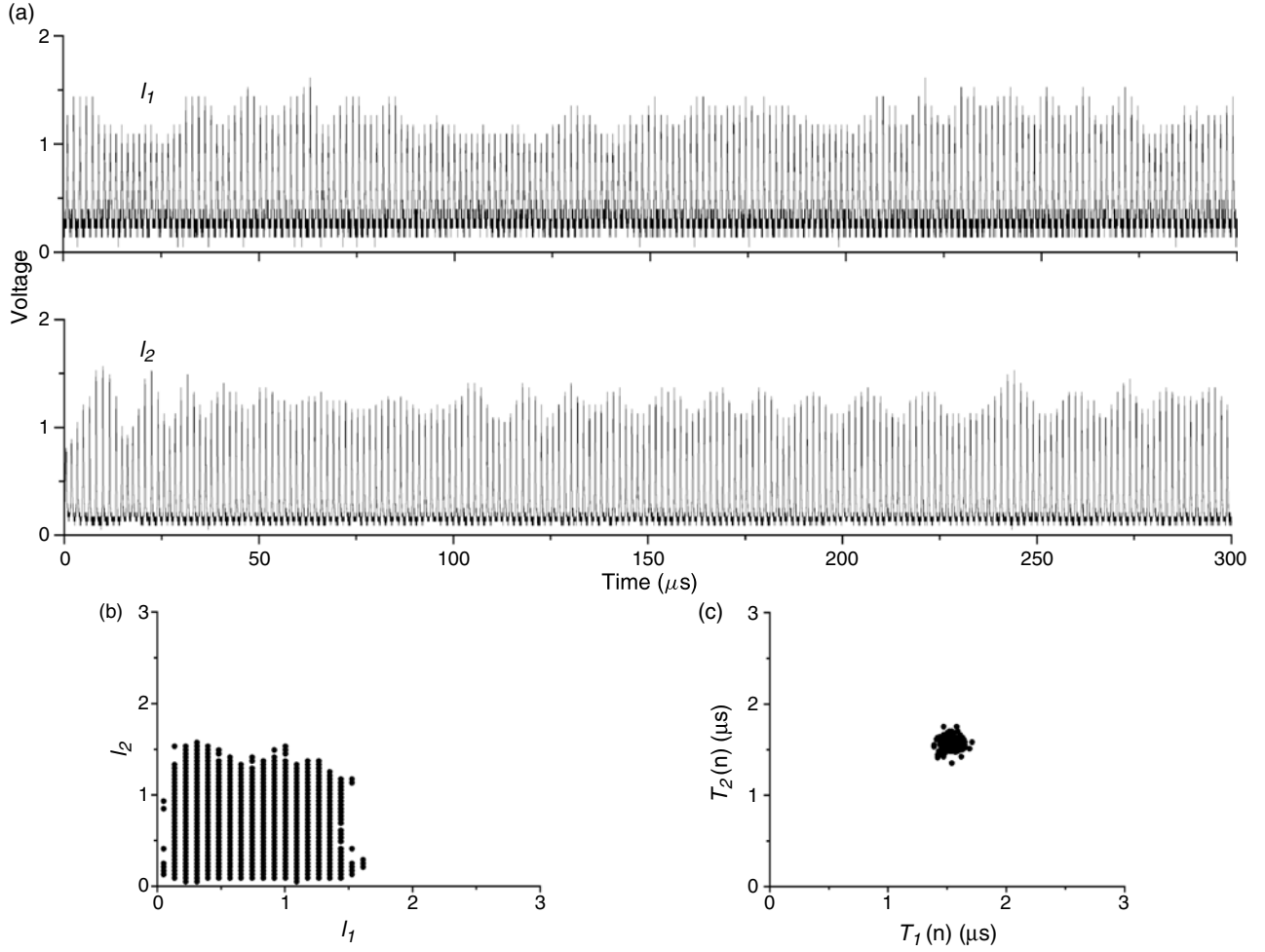
Figure 3. Experimental result of phase-squeezed state. $d \simeq 0.85$ mm. (a) Time evolutions of two lasers, (b) amplitude correlation, and (c) phase correlation.

for laser 2, $T_2(n)$, is plotted against that for laser 1, $T_1(n)$, in figure 2(c). In this case, unsynchronized chaotic fluctuations in both amplitude and phase are apparent, and the two lasers are found to be behaving independently.

When separation between two lasers was decreased to $d = 0.85$ mm, a mutual interaction between the two lasers appeared through transverse field overlap and the phase fluctuations of two lasers are squeezed, while their amplitudes remained uncorrelated, just before the onset of chaos synchronization. Example results are shown in figures 3(a)–(c). We refer to this hereafter as the phase-squeezed state. This phenomenon could be interpreted in terms of a slaving principle: system dynamics is governed by $(\tau \tau_p)^{\frac{1}{2}}$, while the amplitudes are determined by the much shorter timescale of τ_p. Let us examine the phase-squeezed state further by extracting the analytical phase from experimental time series. Using the Hilbert transformation of time series, i.e., Gabor's analytic signal used in the analysis of phase synchronization [8, 9], we calculated the analytic phase correlation of two lasers. The analytic signal V_A and its time average $\langle V_A \rangle$ were calculated by $V_A(t) - \langle V_A \rangle = R_A(t)e^{i\phi(t)}$. Here, $V_A(t) = I(t) + iI_H(t)$ where $I(t)$ is the time series of scalar intensity and I_H is the its Hilbert transform. The dynamic change over time of the difference in analytic phases of the two lasers is plotted in figure 4(a). Here, two signals are

in phase in region A, while they become out of phase in region B after a transient phase-slipping. Phase correlation plots in region A and region B are shown in figures 4(b) and (c). In the phase-squeezed state, the phase difference is not fixed and such relative-phase switching occurs over time, resulting in uncorrelated amplitudes of the two signals.

When d was decreased further, synchronized chaotic states, in which the two lasers exhibited chaotic pulsations with both strong amplitude and phase correlation within allowed errors, are obtained. Results for $d \simeq 0.8$ mm are shown in figures 5(a)–(c).
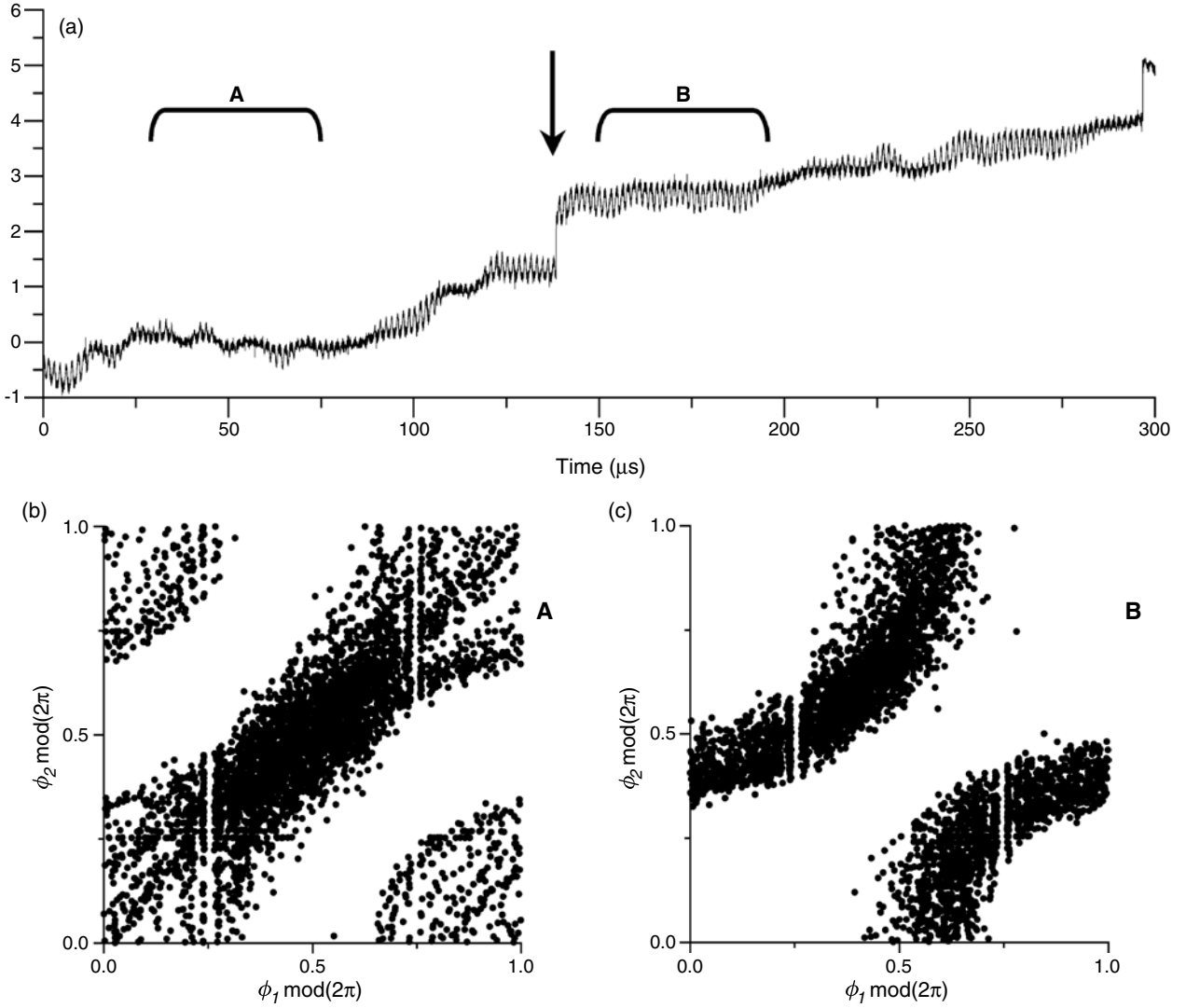
3. Numerical results

3.1. Synchronized chaos

The following model equations are used to be explore the dynamics of coupled lasers subjected to Doppler-shifted light injection:

$$\frac{dE_i}{dt} = N_i E_i + \eta E_{i+1} \cos\theta + m_i E_i(t - t_d) \cos\varphi_i,$$

$$\frac{d\varphi_i}{dt} = \Omega_i - \Omega_{s,i} - m_i[E_i(t - t_d)/E_i(t)] \sin\varphi_i,$$

$$\frac{dN_i}{dt} = [w_i - 1 - N_i - (1 + 2N_i)E_i^2]/K,$$

Figure 4. Analytic phase of two lasers in the phase-squeezed state shown in figure 3. (a) Time evolution of analytic phase difference between two lasers, (b) analytic phase correlation in region A, and (c) analytic phase correlation in region B.

$$\frac{d\theta}{dt} = \Omega_2 - \Omega_1 - \eta(E_1/E_2 + E_2/E_1)\sin\theta,$$

$$i = 1, 2,$$

where E_1 is the normalized field amplitude ($E_3 = E_1$), N_i is the normalized population inversion, $w_i = P_i/P_{i,th}$ is the relative pump power, $\theta = \phi_2 - \phi_1$ is the relative phase of two electric fields, $\Omega_i = \omega_i/\kappa$ is the normalized oscillation frequency ($\kappa \equiv 1/(2\tau_p)$: damping rate of the optical cavity), $\Omega_{s,i} = \omega_{s,i}/\kappa$ is the normalized frequency of the scattered field, φ_i is the phase difference between the lasing field and scattered field fed back to the resonator, m_i is the feedback coefficient, $K = \tau_f \kappa$, and t and t_d are the dimensionless time and delay time normalized by κ. The present system is more complicated than a simple pump or loss modulation and in fact the experimental results are different from those in [5, 22]. This may result from the self-mixing feedback effect which we have explained above. Numerical time series and correlation plots of synchronized chaos are shown in figure 6, assuming $w_{1,2} = 1.05$, frequency detuning of two lasers $\Omega_2 - \Omega_1 = 10^{-5}$, $\eta = -1.382 \times 10^{-4}$, $m_{1,2} = 0.005$,

$\Omega_1 - \Omega_{s,1} = \Omega_2 - \Omega_{s,2} = 2\pi \times 10^{-3}$, and $K = 2 \times 10^{-3}$. The delay time of $t_d = 3$ ns was much smaller than the fluctuation timescale, so we assumed $t_d \ll 1$ (a short-delay limit). The distinctive feature of synchronized chaos states in the present system is that oscillations of the two chaotic lasers are strongly localized in the vicinity of the 'perfect' synchronous state even in the presence of frequency detuning as shown in figure 6, and cannot escape from this state. That is, they are stable *stagnant motions*. It has also been confirmed numerically that phase squeezing occurs when the coupling is reduced, similar to the experimental result shown in figures 3 and 4.

3.2. Statistical properties of different chaotic states

Let us show changes in global statistical feature of dynamic states numerically by varying the coupling coefficient, using such quantities as averaged standard deviations of intensity and phase, and average variation of disorder based on the Shannon entropy.

First, the degree of synchronization is evaluated in terms of average errors of intensity and phase defined as

(a)

(b)

(c)
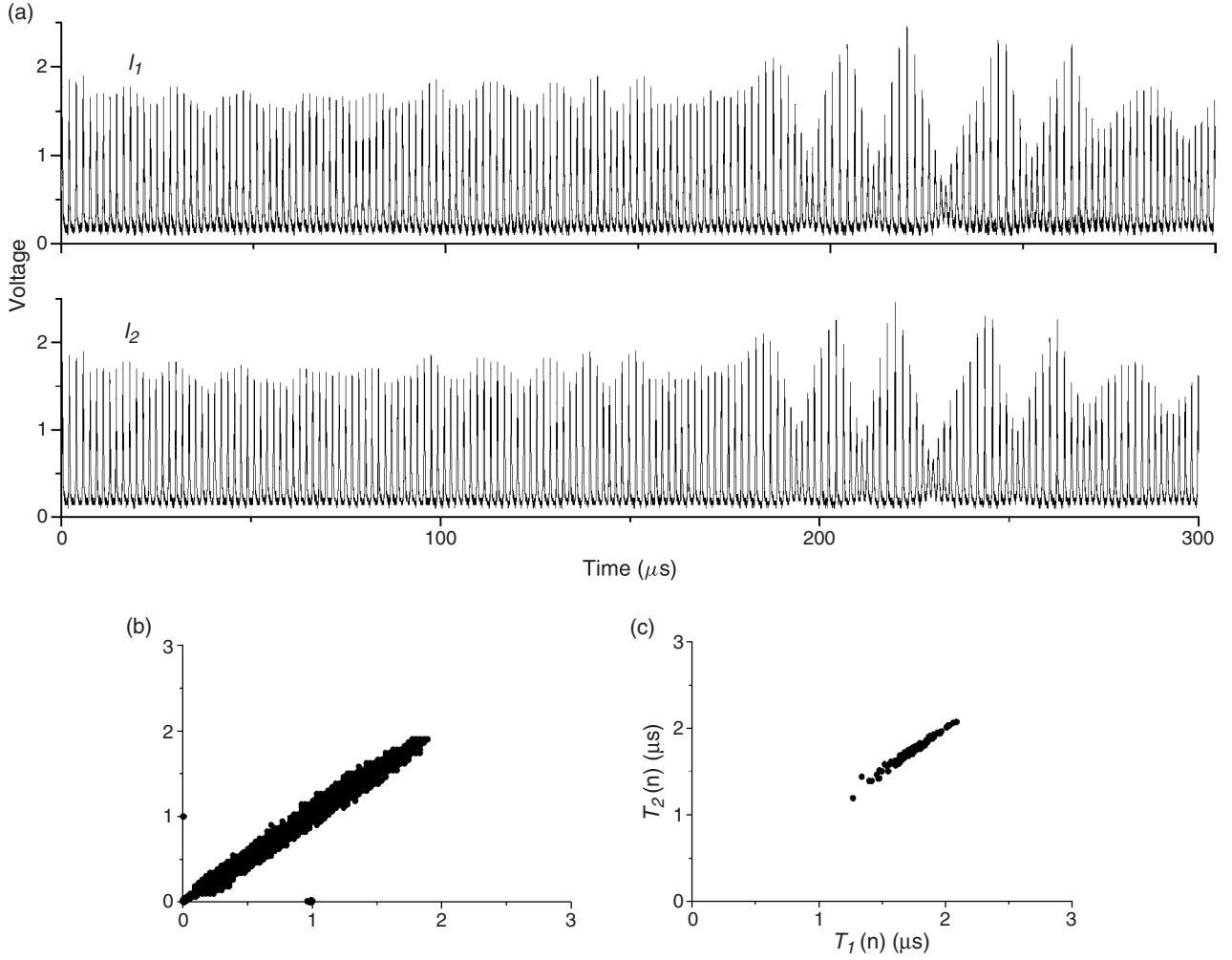
Figure 5. Experimental result of synchronized chaos. $d \simeq 0.8$ mm. (a) Time evolutions of two lasers, (b) amplitude correlation, and (c) phase correlation.

$$\langle \varepsilon_I \rangle = \frac{1}{\Delta T} \int_0^{\Delta T} |E_1(t)^2 - E_2(t)^2| \, dt$$

for the intensity ($\Delta T \gg 1$) and

$$\langle \varepsilon_T \rangle = \frac{1}{M} \sum_{i=1}^{M} |T_1(i) - T_2(i)|$$

for the phase ($M \gg 1$). Calculated results are shown in figure 7(a), in which transition occurs at the coupling $|\eta| \sim 1.38 \times 10^{-4}$ and phase squeezing took place just before the onset of chaos synchronization.

The degree of phase squeezing is identified by the averaged standard deviation of phase defined as

$$\delta_T = \frac{1}{2} \sum_{i=1}^{2} \langle (T_i - \langle T_i \rangle^2) \rangle$$

where $\langle \cdots \rangle$ denotes the time average. To explore more features around the transition, we calculated the average standard deviation of intensity (i.e., energy), defined as

$$\delta_I = \frac{1}{2} \sum_{i=1}^{2} \langle (E_i^2(t) - \langle E_i^2 \rangle)^2 \rangle,$$

as a function of the coupling. Calculated averaged standard deviations of intensity and phase are shown in figure 7(b). It is found that the synchronized chaos shows lower variation of energy, i.e., δ_I, than the unsynchronized chaos. Also note that the averaged standard deviation of phase δ_T decreases rapidly as the system approaches the phase-squeezed state and increases abruptly again in the synchronized state. This parallels the experimental result.

We also calculated the average variation of disorder based on the Shannon entropy defined as

$$\delta_H = \frac{1}{2} \sum_{i=1}^{2} H_i,$$

where $H_i = -\sum_{l=1} P_i(l) \ln P_i(l)$, in which $P_i(l)$ is the probability of the intensity localized within the lth interval during time evolution for laser i ($i = 1, 2$). The calculated δ_H in figure 7(b) implies that when the synchronized chaos occurs a larger disorder is established while the mutual information between the two lasers is increased. This point will be discussed again in the appendix.

From these results, it should be pointed out that a lower variation of energy as well as a higher disorder are required for synchronized chaos to be established in the present system.
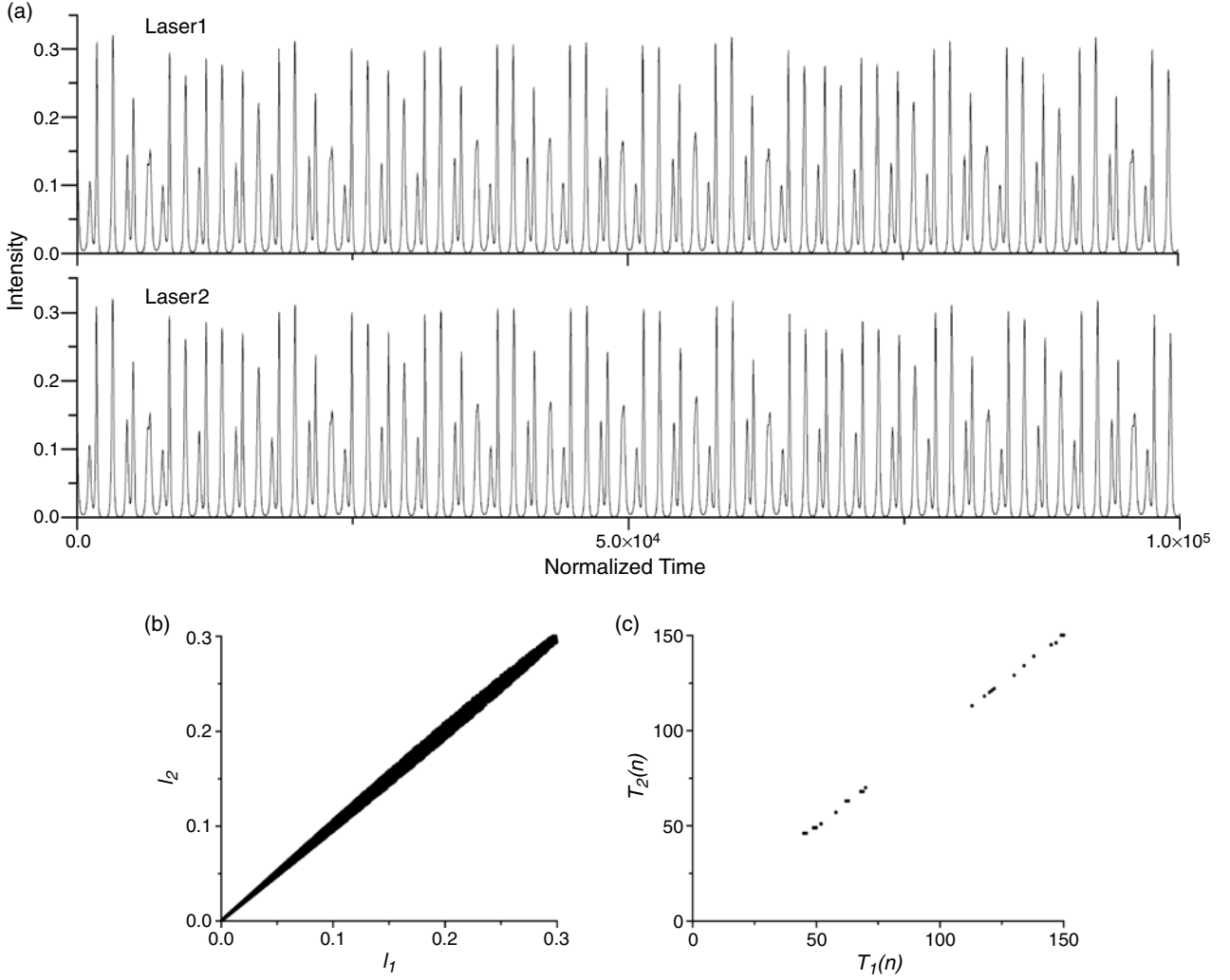
Figure 6. Numerical result of synchronized chaos. Adopted parameter values are given in the text. (a) Numerical time series, (b) amplitude correlation, (c) phase correlation.

This is a significant feature and could be a general characteristic of the synchronization of mutually coupled chaotic oscillators in systems where energy can be defined. At any rate, the nature of synchronized chaos is qualitatively different from that of unsynchronized chaos before the transition.

4. Dynamical characterization of dynamic states

4.1. Singular-value-decomposition analysis

Let us first characterize three dynamic states, i.e., unsynchronized, phase-squeezed, and synchronized states, using the singular-value-decomposition (SVD) analysis [17]. The SVD method is powerful not only for distinguishing noise and chaos but also for evaluating the embedding dimension of chaos. With a phase-space reconstruction on the measured time series, noise will dominate the redundant dimensions by which the noise level can be distinguished. Also, the decay rate of SVD eigenvalue spectra gives a measure of chaos.

Practically, as power is measured, we have a time series $\{P(k\Delta)\}$, where Δ is the time difference between two successive samplings and $k = 1, 2, \ldots, (N + d - 1)$. Here,

d is the embedding dimension for phase-space reconstruction and $(N + d - 1)$ is the total number of data. We can construct a d-dimensional vector $Y(t) = [P(t), P(t + \Delta), \ldots, P(t + (d - 1)\Delta)]$. With those vectors, one can define a trajectory matrix A:

$$A = \begin{bmatrix} P(t) & P(t+\Delta) & \cdots & P(t+(d-1)\Delta) \\ P(t+\Delta) & P(t+2\Delta) & \cdots & P(t+d\Delta) \\ \vdots & \vdots & \ddots & \vdots \\ P(t+(N-1))\Delta & P(t+N\Delta) & \cdots & P(t+(N+d-1)\Delta) \end{bmatrix}.$$

This equation contains all dynamical information. Using the SVD method, the matrix A can be decomposed such that $A = VSU^T$, where V is an $N \times d$ orthogonal matrix, U is a $d \times d$ orthogonal matrix, and S is a $d \times d$ diagonal matrix; i.e., $(V^T V)I_{i,j} = \delta_{i,j}$, $(U^T U)I_{i,j} = (UU^T)I_{i,j} = \delta_{i,j}$, $S_{i,j} = \delta_{i,j}s(i)$, where the index I $(j) = 1, 2, \ldots, d$. The matrix S is the singular-value matrix of A and $s(i)$ is the corresponding singular-value matrix at the ith index. Since $U^T(A^T A)U = S^2$ and $(A^T A)U = S^2 U$, $[s(i)]^2$ are eigenvalues of $(A^T A)$ and U is the corresponding set of eigenvectors. The normalized $[s(i)]^2$ is rearranged in descending order and is called the SVD spectrum [17].
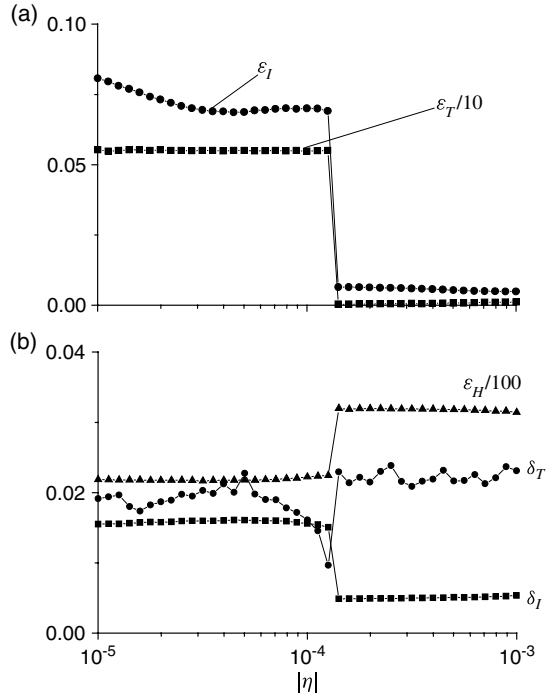
Figure 7. Variations of statistical properties as a function of coupling $|\eta|$. Adopted parameters are the same as figure 6. (a) Average errors for amplitude ε_I and phase ε_T; (b) average standard deviations of amplitude δ_I, phase δ_T, and entropy δ_H.

For the chaotic signal, the SVD eigenvalue spectrum displays two segments when the dimension d is large enough. In the following analysis, we set $d = 100$. The first segment exhibits an experimental decay, that mainly reflects the nature of chaos. The second segment is a straight line (noise floor) which is approximately horizontal. For periodic and quasiperiodic signals, on the other hand, the first segment is replaced by a sudden drop. There is an important property: as the noise contribution is increased, the floor is lifted while the first segment featuring an exponential decay remains unchanged. For a Gaussian white noise, for instance, a flat SVD spectrum appears.

The calculated SVD eigenvalue spectra for different dynamic states corresponding to figures 2 (unsynchronized), 3 (phase squeezed) and 5 (synchronized) are shown in figures 8(a)–(c), respectively. Each SVD spectrum was obtained for the time interval of 4096 data lengths and the shift of 1024 data lengths was introduced for the next calculation. The first segments of the SVD spectra show an exponential decay in the form of $\exp(-\gamma i)$ for all dynamic states (i, index of dimension), indicating that all the dynamic states are nothing other than chaotic states, where i-values are -0.65 (unsynchronized chaos), -0.87 (phase-squeezed state) and -0.69 (synchronized chaos). Note that the constant floor in the second segment in the SVD spectrum decreases as the coupling coefficient increases and the system goes into the synchronized chaos state via the phase-squeezed state. This result implies that the noise contribution decreases when chaos synchronization occurs. In short, the synchronized chaos has been found to be qualitatively different from that of unsynchronized chaos based on the singular-value-decomposition (SVD) analysis of experimental time series.
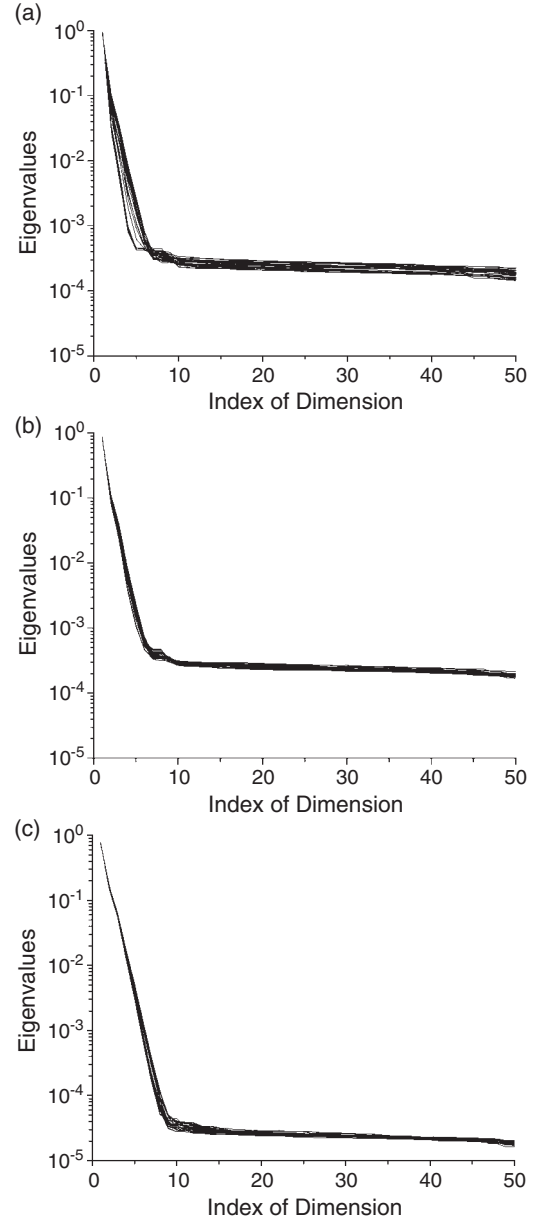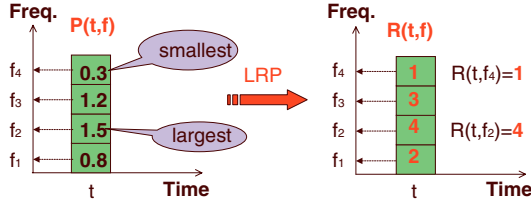

Figure 8. SVD analysis of experimental time series in figures 2–4: (a) unsynchronized chaos, (b) phase-squeezed state, and (c) synchronized chaos.

4.2. Joint time–frequency analysis

Joint time–frequency analysis (JTFA) which expands the signal in both time and frequency domains is widely used to study non-stationary time series. In this subsection, a generalized JTFA featuring a *similarity function* is introduced to identify the correlation of JTFA spectra of two lasers using the experimental time series of unsynchronized, phase-squeezed, and synchronized chaos to reveal correlation portraits in both time and frequency for different dynamic states.

The motivation of the present JTFA is to reveal the crucial factor responsible for the chaotic behaviour, i.e. random switchings among different frequency components of unstable motions ('modes') as time evolves. In fact, from the viewpoint of energy transfer, a complex time series has

**Figure 9.** Schematic illustration of local ranking procedure of JTFA signals.
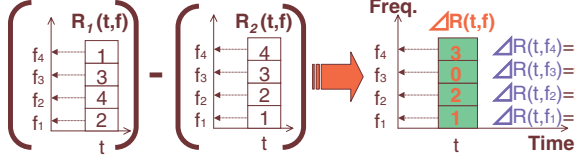
Figure 10. Schematic illustration of rank matching procedure.
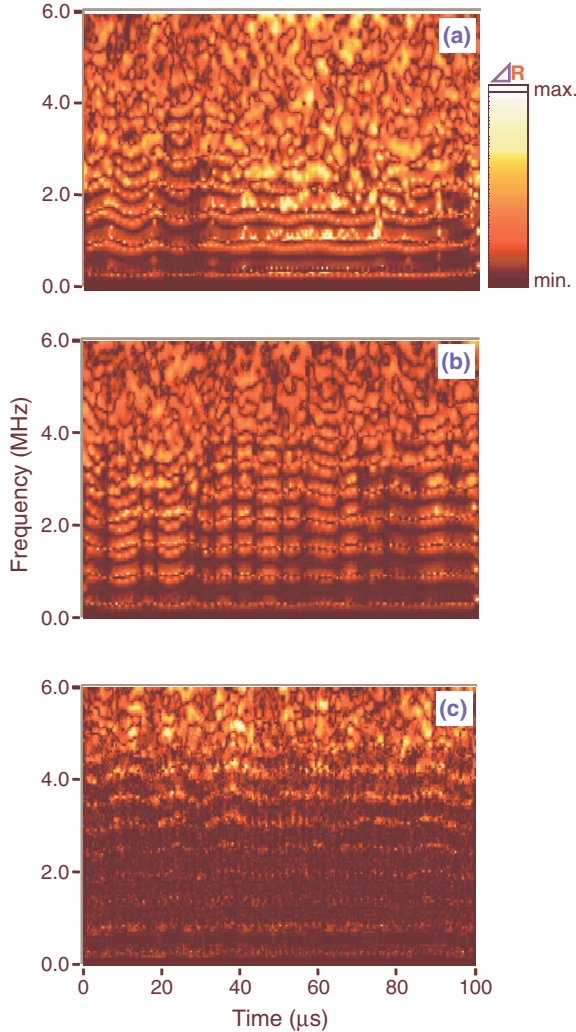
Figure 11. Difference between JTFA signals of two lasers, $\Delta R(t, f)$, as a function of time, calculated by using experimental time series of figures 2–4. (a) Unsynchronized chaos, (b) phase-squeezed state, and (c) synchronized chaos.

inherently large bandwidth and the intensity of the high-frequency component may be so much smaller than that of
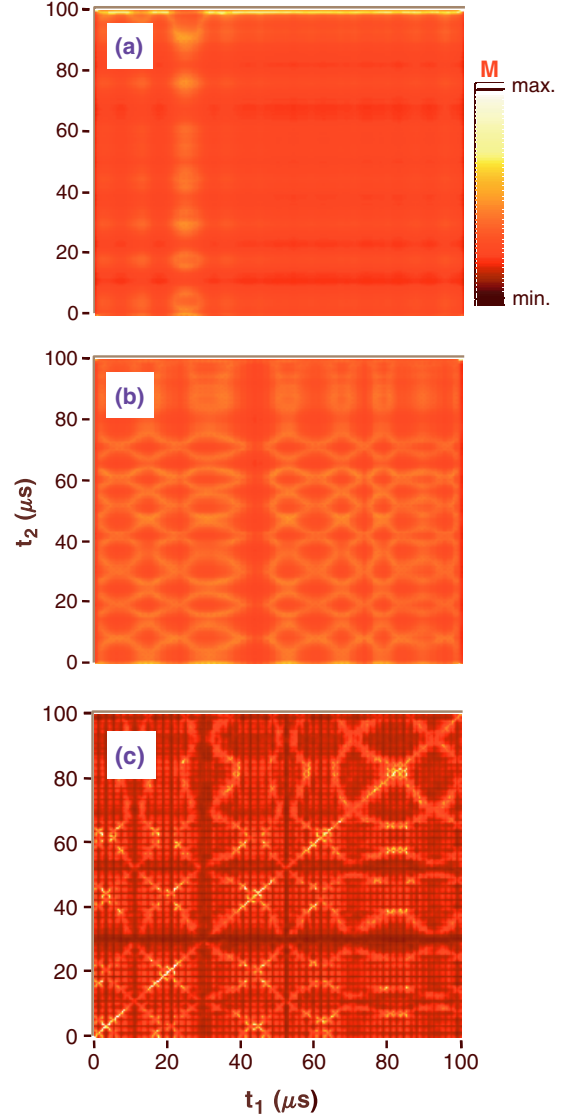
Figure 12. Correlation of JTFA signals of two lasers, $M(t_1, t_2)$, calculated from figure 11. (a) Unsynchronized chaos, (b) phase-squeezed state, and (c) synchronized chaos.

the low-frequency component that the dynamical transitions among modes in the higher-frequency domain are not obvious. Therefore, for the study of complex phenomena such as turbulence and synchronized chaos, the issues of how to identify the dominant mode and subsequently how the interplay of modes proceeds appear to be indispensable and crucial.

The procedure of phase retrieval consists of a number of simple steps. First, the original signals are analysed by the short-time Fourier transform (STFT). The basic idea of STFT applied to a set of time series is to break up the time series via a window function into groups of data and analyse each data segment with Fourier transform to identify the power spectrum for each subset. The sequential calculation identifies how the power spectrum is varying in time. Mathematically, the spectrogram at time t can be expressed as the squared magnitude of the STFT of time series $s(t)$,

$$P(\tau, \omega) = \left| \int s(\tau) h(t - \tau) \mathrm{e}^{-\mathrm{j}\omega\tau} \, \mathrm{d}\tau \right|^2$$

R27

where $h(t)$, in the STFT interpretation of the spectrogram, is the window function to isolate local subsets of the signal data for Fourier analysis. In the present analysis, we have chosen the Hanning window as the window function, i.e., $h(t) = 0.54 + 0.46\cos(\frac{2\pi t}{N-1})$, if $0 \leqslant t \leqslant N$, otherwise $h(t) = 0$ where the window length $N = 64$ samples here. The properties of the time series are scrambled with the window function in the STFT algorithm and how well the adopted window function performs will depend on the characteristic of the signal. The present choice of window function and window length provides a reasonable compromise between time and frequency resolution, although other choices may be more suitable for different purposes. In addition, to remove possible numerical artifacts caused by the dc value in joint time–frequency flow, the dc parts of signals are removed.

The second ingredient of this method presented here is the local ranking procedure illustrated in figure 9, which is to rank the intensity of the spectrogram distributed over frequency domain at an instant of time. We define the rank of the smallest intensity of spectrogram associated with the frequency component f_i at one instant T to be unity, i.e. $R(T, f_i) = 1$ shown in figure 12, the second smallest intensity related to the frequency component f_j to be two, i.e. $R(T, f_j) = 2$, and so on. In other words, the higher the value of the rank corresponding to the frequency f, the greater the contribution that frequency f devotes to the instant behaviour. As a result, we can obtain a ranking distribution: $R(t, f)$, where t is the time and f is the frequency. (We will denote by $R_l(t, f)$ the lth signal hereafter.) By definition, the energy density distribution, which represents the exact magnitude of power at the respective frequency, is mapping into the rank distribution. The relative ranking of frequency components, instead of the absolute power spectral density, can serve as a useful tool to visualize how the frequency component changes as time goes on. A direct estimate of rank matching, which corresponds to the correlation of two JTFA signals, can be easily achieved by

$$\Delta R = |R_1(t, f) - R_2(t, f)|.$$

Here, ΔR is equal to zero when the ranks of frequency f at time t are the same as shown in figure 10, while a nonzero value implies a different nature of the two signals in the Fourier components. Another measure similar to the visibility, $V = |\frac{P_{s1} - P_{s2}}{P_{s1} + P_{s2}}|$, can also reveal the difference between the STFT spectra of two signals $s_1(t)$ and $s_2(t)$, but ΔR is found to be a more effective representation.

Figures 11(a)–(c) show various $\Delta R(t, f)$ distributions for unsynchronized, phase-squeezed, and synchronized signals, respectively. The rank differences fluctuate violently over almost the whole frequency domain in the unsynchronized case. In the phase-squeezed case, the rank difference decreases in the frequency domain $\leqslant 5$ MHz and changes over time, featuring the inherent periodicity. In the synchronized case, the time evolution of ranks in the lower-frequency regime decreases further to be almost in step while the others in the higher-frequency domain still stay in high discordance. These results suggest that lower-frequency modes play a dominant role for synchronization, while the higher-frequency modes are not active in this system. In other words, high-frequency modes are not well correlated even if the chaos synchronization is established.

The third step is to introduce a similarity function to characterize the pattern similarity over the whole frequency domain. We define the similarity function as

$$M(t_1, t_2) = \frac{1}{\Sigma_l' |R_1(t_1, f) - R_2(t_2, f)|},$$

where the prime means a summation over all f except for $R_1(t_1, f) - R_2(t_2, f) = 0$. Let us consider two signals: $s_1(t_1)$ and $s_2(t_1 + \Delta t)$, where $\Delta t = t_1 - t_2$ is the time delay between $s_1(t)$ and $s_2(t)$. To be more informative, it is useful to take a view on the $[t_1, t_2]$ space constructed from the similarity function M. By definition, it can be expected that $M(t_1, t_2)$ has the maximum value when $t_1 = t_2$, if $s_1(t)$ and $s_2(t)$ are synchronized, while the largest values of $M(t_1, t_2)$ are located on the line $t_1 = t_2 + n\Delta t$ when both signals are periodic in a time interval Δt (n integer). The relative phase is encoded in the relative position (difference) of labelled points, such as the maximum, the minimum, or any other significant point (e.g., turning point) in the time flow. Although the phase information is unknown in the power spectrogram, the M picture gives us information on the relative phase of two signals as well. This means that we can deduce a phase portrait between two signals. In short, deviations of the maximum values from the $t_1 = t_2$ line are caused by the phase difference of the intensities of the two signals. In contrast, in the case of two white noises, the M picture indicates an almost totally uniform distribution because of the random distributed frequency spectrum. However, broad-bandwidth signals from chaotic systems are usually complex and complex M portraits are expected to appear.

The measure of similarity for the unsynchronized chaos is shown by figure 12(a). Values of the similarity function for unsynchronized signals are almost uniform in the $[t_1, t_2]$ space. This is due to the fact that the patterns of the rank functions of the two signals are uncorrelated and thus they are averaged out to be constant. Let us now attempt to extend the above analysis to the case of two signals in the phase-squeezed state. In this case, the amplitudes of the two lasers are in independent motion, while their phase fluctuations are squeezed so that the pulsation periods tend to become uniform. The result is shown by figure 12(b). Compared with the unsynchronized case, it is obvious that the pattern constructed by the rank function in the $[t_1, t_2]$ space displays a very different structure: namely netlike structure. The similarity fluctuation for the phase-squeezed chaos is converged to form some structural flows instead of a uniform distribution and these larger values of the similarity function construct some regular flows in column and row directions. From the viewpoint of the time–frequency spectrum, the magnitude of phase fluctuation corresponds to the difference in times where the similar frequency components appear. As a result, maximum values of the matching function for two phase-squeezed signals will appear sometimes far from and sometimes near to the line $t_1 = t_2$, reflecting almost uniform pulsation periods of the two signals. For the synchronized chaos, as one can see in figure 12(c), a bright matching line corresponding to $t_1 = t_2$ and some irregular, but self-similar, patterns are apparent on the $[t_1, t_2]$ space. The highly bright line $t_1 = t_2$ means that the JTFA spectra of the two chaotic time series are almost identical, i.e. these two time series are synchronized. Nevertheless, astonishingly, a mirror symmetry with self-similar M pattern has been established in synchronized chaos.
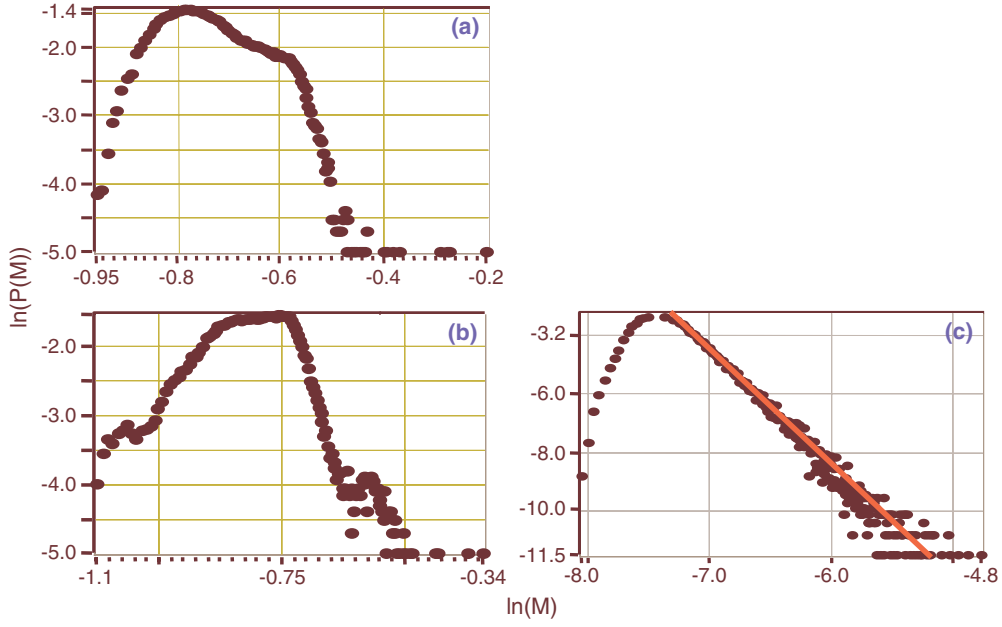
Figure 13. Probability distribution $P(M)$ of M for different dynamic states calculated from figure 12. (a) Unsynchronized chaos, (b) phase-squeezed state, and (c) synchronized chaos.

The occurrence of self-similar M distribution shown in figure 12(c) suggests that some power law scaling is embedded in the M portrait of synchronized chaos. To explore the feature, we partition the range of M with 500 intervals and the histogram of M is calculated for each dynamic state. Results are shown in figure 12. When the chaos synchronization is established, a power law probability distribution of M obeying $P(M) \propto M^{-\alpha}$ with the exponent $\alpha = 4.05 \pm 0.21$ appears for large M as shown in figure 13(c), reflecting the self-similarity. For small M, on the other hand, a quasi-exponential law with $P(M) \propto e^{\beta M}$, where β is a large number (here $\beta \simeq 10^4$), takes place. The minimum value of M is nothing but a signature of noise level inherent in real synchronized signals. As for unsynchronized and phase-squeezed states, on the other hand, no scaling relation is identified as shown in figures 13(a) and (b).

The histogram of M distribution featuring two different scales, as well as different scaling laws, is not limited to the case of synchronized laser chaos here. Indeed, the inherent two-scaling behaviour also holds in the case of the Lorenz chaos. As shown in figures 14(a) and (b), a time series generated from the classic Lorenz chaos with model equations $dx/dt = -10(x - y)$, $dy/dt = -xz + 28x - y$, $dz/dt = xy - \frac{8}{3}z$ and a copy of the same time series subjected to noise were used to generate the M and its histogram. To reveal the fine structure, we removed the large value M at $t_1 = t_2$ and used a partition into 3000 intervals. Exactly the same self-similarity is found to appear for the Lorenz chaos in the M distribution as well as the histogram where the exponent $\alpha = 2.04 \pm 0.17$. It is worthwhile to note that although the pattern in phase portrait may change as time evolves, the exponent value remains the same. In contrast, the power law distribution was destroyed as synchronized chaos disappeared due to the disappearance of self-similarity.
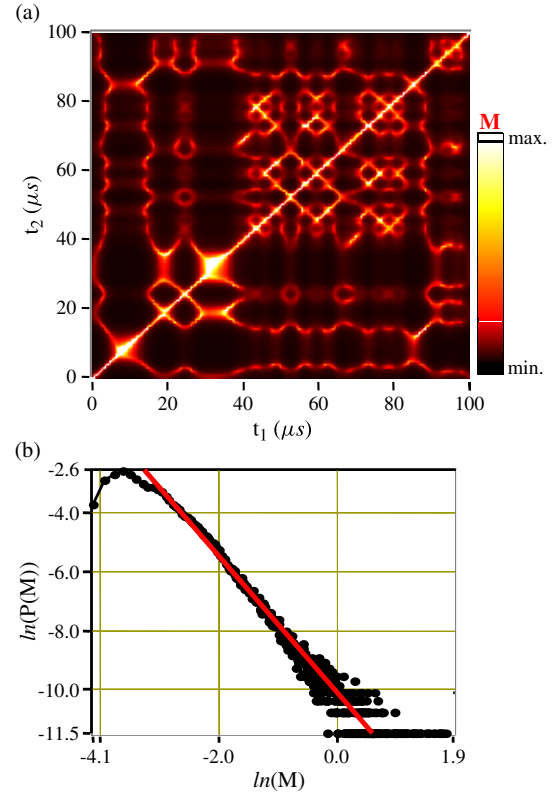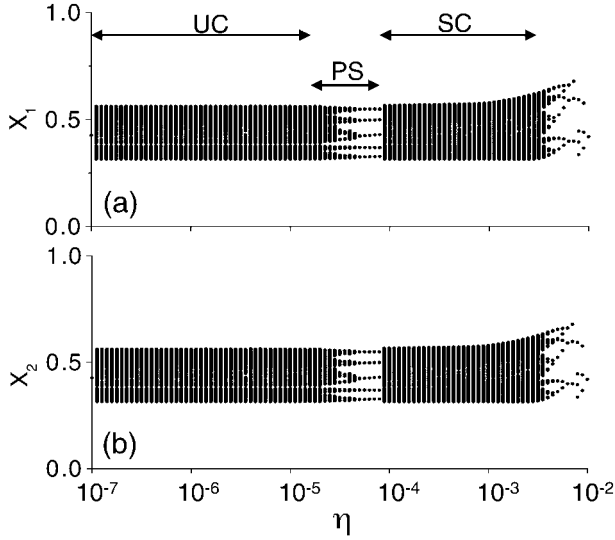

Figure 14. Numerical result for Lorentz chaos. (a) Correlation of Lorenz chaos and Lorenz chaos with noise, (b) probability distribution $P(M)$ of M.

5. Conclusion

We experimentally examined synchronized chaos in two coupled microchip lasers subjected to self-mixing feedback.

Figure A.1. Numerical bifurcation diagrams of two lasers as a function of coupling $|\eta|$. Adopted parameters are the same as in figure 6.

A transition from an unsynchronized chaos to a synchronized chaos via a phase-squeezed state has been found by intensity and phase correlation analysis of long-term experimental time series. Theoretical model equations of coupled laser arrays with frequency-shifted feedback have been presented and a key feature of the experimental results has been reproduced numerically. Global statistical properties of these dynamic states including averaged standard deviations of intensity and phase, as well as the averaged variation of disorder based on the Shannon entropy, have been examined as a function of coupling coefficient between two lasers. The averaged standard deviation of intensity has been shown to decrease abruptly as the system goes into the synchronized chaos state. On the other hand, the average variation of disorder has been shown to increase in the synchronized chaos state.

The dynamical characterization of three dynamic states has been carried out using SVD and JTFA methods. The noise contribution to chaotic dynamics has been shown to decrease as the coupling coefficient increases and the system goes into the synchronized chaos state from SVD analysis of experimental time series. A local ranking procedure emphasizing the distribution of dominant spectral components has been introduced to calculate the matching function ΔR which compares the correlation of two signals in the time–frequency domain. We have applied this function to JTFA of experimental data sets of unsynchronized, phase-squeezed and synchronized chaos in mutually coupled lasers. The results showed that during the route from unsynchronized chaos, through the phase-squeezed state, to synchronized chaos, the level of synchronization was governed by the lower-frequency components of chaotic motions. We have also shown the potential of the matching function for retrieving the phase relationship between two correlated signals. By introducing the similarity function M, which indicates the time correlation of two JTFA signals, a netlike pattern on the M portrait due to the establishment of fixed phase relationship has been found to appear in the phase-squeezed state. The mirror

symmetry structure with self-similarity has been identified in synchronized chaos, in which the power law scaling is established for the probability distribution of M. The influence of noise and/or the other unsynchronized factors has been characterized by the quasi-exponential law.

Appendix. Chaotic itinerancy in the vicinity of chaos synchronization

In this appendix, we demonstrate a random switching between phase-squeezed states and synchronized states which is observed numerically without any external noise when the coupling strength is set near the boundary between these two dynamic states. This provides another example of chaotic itinerancy which often occurs in complex systems in a wide range of disciplines.

Example intensity bifurcation diagrams of mutually coupled lasers 1 and 2 are shown in figure A.1, where unsynchronized, phase-squeezed, and synchronized chaos states are indicated by **UC**, **PS**, and **SC**, respectively, where adopted parameter values are the same as those for figure 6. Calculations were carried out by plotting E_i^2 as $|\eta|$ was increased very slowly in time. Here, it should be noted that detailed bifurcation structures critically depend on starting initial conditions for calculating bifurcation diagrams although the three dynamic states appear in the same regions as figure A.1, independently of initial conditions. This implies that there coexist many attractors in the high-dimensional phase space. For the present calculation, each laser exhibits a similar (not exactly the same) subharmonic bifurcation cascade in the transition process from the unsynchronized chaos to the synchronized chaos, at which phase squeezing takes place. While in the synchronized state, each laser shows exactly the same inverse subharmonic bifurcation cascade as the coupling coefficient is increased.

Let us investigate dynamic behaviours occurring near the boundary between phase-squeezed and synchronized states indicated by the arrow in figure A.1. A typical example of temporal evolutions of the two lasers is shown in figure A.2, where $|\eta| = -1.3725 \times 10^{-4}$ was assumed. It is obvious that the two lasers exhibit switchings between the two states, **SC** and **PS**, via transient unsynchronized states, **UC**. This manifests itself in chaotic itinerancy occurring near the boundary between **SC** and **PS**. Example phase correlation plots $T_1(n)$ versus $T_2(n)$ for the two states, **SC** and **PS**, are shown in figures A.3(a) and (b). In the present case, the two lasers exhibit nearly period-six-cycle pulsations whose phase correlation plot features six localized data point groups as shown in figure A.3(b), in which phase fluctuations in each group are squeezed.

The numerically generated chaotic itinerancy is characterized by using the information-theoretic quantity of time-dependent 'coarse-grained' information transfer rate (CITR) and information circulation between the coupled chaotic oscillators proposed by Palus *et al* [19] and modified by Otsuka *et al* [20, 21]. This quantity can effectively identify the amount and the direction of information flows between two chaotic oscillators.
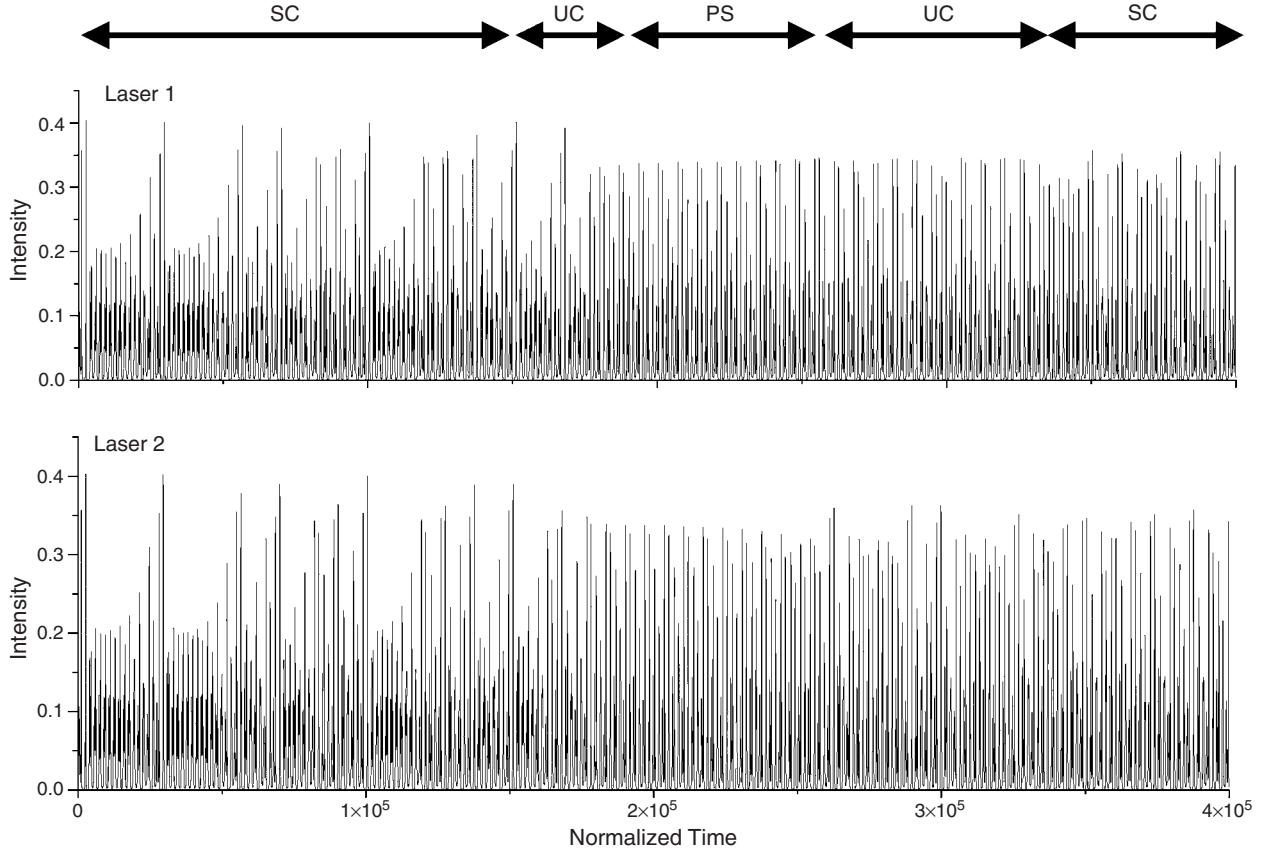
Figure A.2. Chaotic itineracy near the boundary between the phase-squeezed state and synchronized chaos.
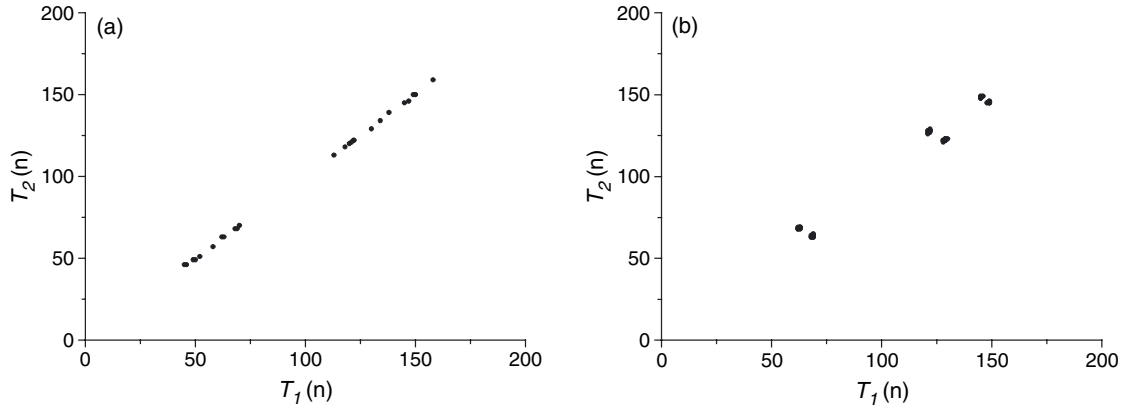
Figure A.3. Phase correlation of two signals. (a) Synchronized chaos region in figure A.2; (b) phase-squeezed region in figure A.2.

The information circulation, that is the net information flows between two time series X and Y, is defined as

$$T_{X,Y} = T_{X \to Y} \to T_{Y \to X},$$

where

$$T_{X \to Y} = \frac{1}{\tau^*} \sum_\tau S(Y, Y_\tau | X) - \frac{1}{\tau^*} \sum_\tau S(Y, Y_\tau),$$

is the information transfer rate from a time series $X = \{x(t)\}$ to $Y = \{y(t)\}$, and $S(Y, Y_T)$ is the self-mutual information for Y, i.e., a measure of the information that Y is able to provide about $Y_\tau = \{y(t+\tau)\}$ (or of the predictability of $Y_\tau = \{y(t+\tau)\}$ given

by Y). $S(Y, Y_T | X)$ is the conditional self-mutual information of the time series X given the time series Y. τ^* is the first local minimum of $S(Y, Y_\tau)$. When $T_{X,Y} > 0$ (<0), the information flow is from $X(Y)$ to $Y(X)$. Figure A.4 shows calculated information flows between the two lasers using the time series shown in figure A.2. It is evident from this figure that the information flow rates, $|T_\rightleftharpoons|$, become larger in the synchronized chaos than those in the phase-squeezed state and the transient unsynchronized state as shown in figure A.4(a), while almost balanced bidirectional information flow is established between two lasers in all dynamic states over time, i.e., $T_{X,Y} \simeq 0$, as shown in figure A.4(b). The increase in the amount of information which is transferred between
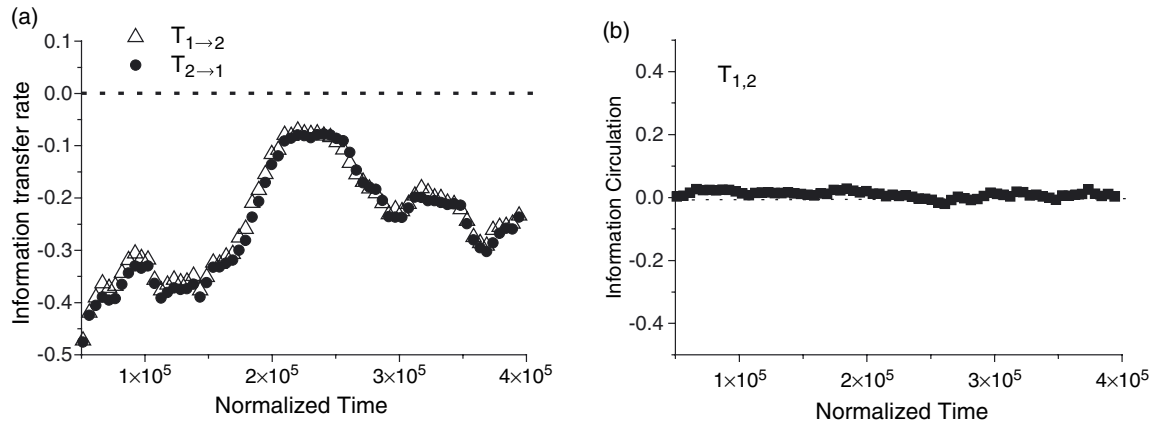
Figure A.4. Information-theoretic characterization of chaotic itineracy shown in figure A.3. (a) Information transfer rates; (b) information circulation.

two lasers in the synchronized state parallels the increase in Shannon entropy in the synchronized state shown in figure 6.

References

[1] Gaponov-Grekhov A V, Rabinovich M I and Starobinets I M 1984 *Pis. Zh. Eksp. Theor. Fiz.* **39** 561
[2] Pecora L M and Carrol T L 1990 *Phys. Rev. Lett.* **64** 821
[3] VanWiggeren G D and Roy R 1998 *Science* **279** 1198 and references therein
[4] Winful H G and Rahman L 1990 *Phys. Rev. Lett.* **65** 1575
[5] Roy R and Thornburg K S 1994 *Phys. Rev. Lett.* **72** 2009
[6] Rulkov N F, Sushchik M M, Tsimring L Sh and Abarbanel H D I 1995 *Phys. Rev.* E **51** 980
[7] Kocarev L and Parlitz U 1996 *Phys. Rev. Lett.* **76** 1816
[8] Rosenblum M G, Pikovsky A S and Kurtz J 1996 *Phys. Rev. Lett.* **76** 1804
[9] Rosa E Jr, Hayes S and Grebogi C 1997 *Phys. Rev. Lett.* **78** 1247
[10] Rosenblum M G, Pikovsky A S and Kurtz J 1997 *Phys. Rev. Lett.* **78** 4193
[11] Koryukin L V and Mandel P 2002 *Phys. Rev.* E **65** 026201
[12] Masoller C 2001 *Phys. Rev. Lett.* **86** 2782
[13] Sivaprakasam S, Shahverdiev E M, Spencer P S and Shore K A 2001 *Phys. Rev. Lett.* **87** 154101
[14] Otsuka K, Ohtomo T, Maniwa T, Kawasaki H and Ko J Y 2003 *Chaos* **13** 1014
[15] Otsuka K, Kawai R, Hwong S L, Ko J Y and Chern J L 2000 *Phys. Rev. Lett.* **84** 3049
[16] Otsuka K 1999 *Nonlinear Dynamics in Optical Complex Systems* (Dordrecht: Kluwer–Academic)
Otsuka K 2003 Chaotic itinerancy *Chaos* **13** 926 (Focus issue)
[17] Lih J S, Ko J Y, Chern J L and Jiang I M 1997 *Europhys. Lett.* **40** 7
[18] Lih J S, Chern J L and Otsuka K 2002 *Europhys. Lett.* **57** 810
[19] Palus M, Komarek V, Hrncir Z and Sterbova K 2001 *Phys. Rev.* E **63** 046211
[20] Otsuka K, Ko J Y, Ohtomo T and Ohki K 2001 *Phys. Rev.* E **64** 056239
[21] Otsuka K, Ohtomo T, Yoshioka A and Ko J Y 2002 *Chaos* **12** 678
[22] Fabiny L, Colet P, Roy R and Lenstra D 1993 *Phys. Rev.* A **47** 4287
[23] Otsuka K, Ko J Y and Kubota T 2001 *Opt. Lett.* **26** 638
Ko J Y, Otsuka K and Kubota T 2001 *Phys. Rev. Lett.* **86** 4025